A novel blue crab chitosan/protein composite hydrogel enriched with carotenoids endowed with distinguished wound healing capability: In vitro characterization and in vivo assessment

Marwa Hamdi, Amal Feki, Sana Bardaa, Suming Li, Sakthivel Nagarajan, Manel Mellouli, Tahia Boudawara, Zouheir Sahnoun, Moncef Nasri, Rim Nasri

A novel blue crab chitosan/protein composite hydrogel enriched with carotenoids endowed with distinguished wound healing capability: *In vitro* characterization and *in vivo* assessment

Marwa Hamdi[a,*], Amal Feki[a], Sana Bardaa[b], Suming Li[c], Sakthivel Nagarajan[c], Manel Mellouli[d], Tahia Boudawara[d], Zouheir Sahnoun[b], Moncef Nasri[a], Rim Nasri[a,e]

[a] *Laboratory of Enzyme Engineering and Microbiology, University of Sfax, National Engineering School of Sfax, Sfax, Tunisia*
[b] *Laboratory of Pharmacology, Faculty of Medicine of Sfax, University of Sfax, Tunisia*
[c] *European Institute of Membranes, UMR CNRS 5635, University of Montpellier, Montpellier Cedex 5, France*
[d] *Laboratory of Anatomopathology, CHU Habib Bourguiba, University of Sfax, Sfax, Tunisia*
[e] *Higher Institute of Biotechnology of Monastir, University of Monastir, Monastir, Tunisia*

Keywords:
Blue crab chitosan
Protein isolate
Composite hydrogels
In vitro assessment
Wound healing

This work aimed to the development of chitosan and protein isolate composite hydrogels, for carotenoids-controlled delivery and wound healing. By increasing the concentration of the protein isolate, chitosan hydrogels were more elastic at a protein isolate concentration not exceeding 15% (*w*/w). Chitosan-protein isolate composite hydrogels revealed low cytotoxicity towards MG-63 osteosarcoma cells. Thanks to its appropriate structural, swelling and mechanical resistance properties, chitosan hydrogel (3%; *w*/*v*), reinforced with 15% (*w*/w) of protein isolate, was selected for the carotenoids *in vitro* release study. Release profiles, show delivery patterns, where carotenoids were more barely released at a pH 7.4 medium ($p < .05$), compared to more acidic microenvironments (pH 4.0 and pH 2.0). Thus, developed hydrogels could be applied as pH-sensitive intelligent carriers, for drugs-controlled release, with interesting antioxidant abilities. The *in vivo* healing potential of hydrogels in rats' models was further studied. Topical application of hydrogel-based patches allowed the acceleration of wound healing and the complete healing, for composite hydrogel enriched with carotenoids.

1. Introduction

Hydrogels are defined as solid and translucent systems or materials. Unlike biofilms, hydrogels are essentially made of polymers and are able to retain up to 90% of water in their networks. This specificity makes it possible to apply them in the medical field for the delivery of drugs and molecules of therapeutic interest or for treating skin wounds, *etc.* [1].

Nowadays, drug administration is a very interesting subject. Targeted drug delivery aims to improve the concentration of the drug in specific sites relative to others, and to cause widespread, localized, targeted and protected interactions with damaged tissues [2]. Drug release occurs from delivery systems through various mechanisms, including diffusion, swelling, erosion, and stimuli-based pathways [3]. Among interesting natural substances studied in this context, carotenoids are widely applied in several cosmetics and pharmaceutical industries, because of their various bioactivities, mainly antioxidant, antimicrobial, anticancer, immunomodulatory, antidiabetic and anti-inflammatory effects [4].

Moreover, one of the, currently, recurring problems, which requires careful consideration, is skin damage. Wound healing is based on repairing the integrity of the damaged tissue by preventing dysregulated homeostasis [5]. An ideal dressing should preserve moisture at the wound interface, allow for gas exchange, provide a barrier against pathogens and eliminate additional exudates, ensure solubilization of growth factors and/or antimicrobial agents, and support growth of fibroblasts, be non-allergenic, non-adherent, non-toxic and eliminated without trauma [6]. Low adhesion to the wound surface and oxygen exchange capacity further promote healing [7]. Natural skin substitutes have increasingly attracted the attention of researches, being efficient in accelerating epithelialization and enhancing wound healing cascade [8]. Recently, natural biomaterials, due to their biocompatibility, have

* Corresponding author at: Laboratory of Enzyme Engineering and Microbiology, University of Sfax, National Engineering School of Sfax, B.P. 1173, 3038 Sfax, Tunisia.
E-mail address: marwahamdi50@yahoo.fr (M. Hamdi).

been fully preferred as encouraging alternatives for wound healing remedies, in medicine [9].

Chitosan in the hydrogel form meets these requirements. Indeed, dressings for wound healing based on chitosan exhibit a cluster of unique properties, including the hemostatic properties [10], biodegradability [11] and antimicrobial potential [12]. Actually, chitosan displays antibacterial activity already observed at low concentrations against various pathogens [13] and can be used in various types of formulations such as gels, films or nanoparticles, hence its wide use in the fields medical and veterinary as a promoter of wound healing. Hydrogels are suitable for wounds healing because of their ease of administration, protection, water retention and oxygen permeability [14].

Chitosan can be conveniently applied as a viscous liquid during gelation upon application to the wound surface [15], as dry sponges, films or powders that hydrate rapidly by exudate absorption, forming a chitosan hydrogel at the wound surface [13,16,17], thus the possibility of promising dressing materials design based on chitosan and its derivatives. Their high biocompatibility, biodegradability, excellent antimicrobial activity, non-toxicity and moisturizing capacity prove that chitosan and its derivatives are an outstanding material for wound healing [18].

The first objective of this work was, thus, the conception of bioinspired hydrogels based on blue crab chitosan, reinforced with protein isolate and enriched with carotenoids, extracted from the same species. Indeed, many studies have focused on gelation of proteins because of their interesting textural properties and their ability to trap molecules of interest in the gel networks [19,20]. Carotenoids, from blue crab shells, were loaded into the hydrogels network not only as bioactive additives to improve hydrogels antioxidant activities, but also as drug model for the *in vitro* drug delivery assessments. Moreover, the present study describes the possibility of application, in the dermopharmacy, of the developed composite hydrogels, by studying their wound healing potential, topically on a rat model in comparison with a reference (MEBO®).

2. Materials and methods

2.1. Materials and reagents

Chitosan (Cs), with molecular weight (Mw) of 115 kDa, acetylation degree (AD) of 8% and intrinsic viscosity [η] of 3432 mL/g, was extracted from blue crab shells as reported in our previous study, following a three steps procedure (chemical demineralization, enzymatic deproteinization and chemical deacetylation) [21]. Carotenoids (Cds), containing 4243 μg/g extract of total carotenoids, with a recovery yield of 84%, were extracted from blue crab shells as described in our earlier work, based on the maceration approach, using the binary organic system Hexane/Isopropanol (1/1, *v*/v) [22].

MEBO®, used as a reference drug for the wound healing tests, was purchased from a local pharmacy. Isopropanol and n-hexane were purchased from LobaChemie (Pvt. Ltd., India). Ethanol (96% vol, CAS 64–17-5), phosphate buffered saline (PBS) (P4417), 3-(4,5 dimethylthiazol-2-yl)-2,5-diphenyl tetrazolium bromide (MTT, 98%, CAS 298–93-1) were purchased from Sigma-Aldrich Chemical Co. (St. Louis, USA). MEM alpha medium (Gibco 12,571–063), dimethyl sulfoxide (DMSO) (BDH Prolabo 23,486.297), foetal bovine serum (FBS) (Eurobio CVFSVF00–01), penicillin/streptomycin (Gibco 15,140–122) and 0.05% trypsin-EDTA (Gibco 25,300–054) were used for cell cultures. The other used chemical reagents, purchased from Sigma-Aldrich, were of analytical grade and employed as received without further purifications.

2.2. Animals

Male Wistar rats, having a body weight 147.23 ± 10.59 g, were purchased from the Faculty of Science of Gabes-Tunisia. Each rat was housed separately in clean polyethylene cage under standard environmental conditions of relative humidity (60–70%) and temperature (22–25 °C). The animals were given water and standard pellet diet throughout the wound healing experiments.

2.3. Design of blue crab chitosan-protein isolate composite hydrogels

2.3.1. Blue crab protein isolate extraction and characterization

To prepare blue crab protein isolate (PI), based on the pH-shifting approach, muscle was homogenized with cold water (4 °C) at a water/muscle ratio of 9:1 (*v/w*), following the method detailed by Chaijan et al. [23]. In order to solubilize muscle proteins, the mixture was adjusted to pH 11.5 with NaOH 2 N solution, gently stirred for 60 min and then centrifuged at 8000 *g* for 20 min at 4 °C. Soluble proteins in the supernatant were, thereafter, precipitated by adjusting the pH to proteins isoelectric point (pHi) 5.0 with HCl 2 N solution. Precipitated proteins were collected by centrifugation, at 8000 *g* for 20 min, followed by the adjustment of pH to 7.0 using NaOH 2 N solution. Protein isolate was finally freeze-dried at a temperature of −50 °C and a pressure of about 121 mbar (Moduloyd-230 freeze-dryer, Thermo Fisher Scientific, USA) and thereafter stored at −20 °C for its subsequent use.

PI was characterized in terms of extraction (*w*/w; in dry weight basis) yield, moisture and ash contents [24] and total nitrogen content using Kjeldahl method [24]. Crude protein was estimated by multiplying total nitrogen content by the factor of 6.25. Fat was determined gravimetrically after Soxhlet extraction of dried samples with hexane [25]. All measurements were expressed on a dry weight basis and were performed in triplicate.

Functional properties of PI were, further, determined, considering its solubility [26], water/fat binding capacities [27]. Foaming [28] and emulsifying [29] properties of PI were, moreover, investigated.

2.3.2. Hydrogels preparation

Hydrogels were prepared based on the freezing/thawing approach described by *Duan* et al. [30]. Briefly, Cs and PI were dissolved in an alkaline solution (4.5 wt% LiOH, 7.5 wt% KOH and 8.5 wt% urea) at different PI to Cs mass ratios (2, 5, 10, 15, 20 et 50%; *w*/w Cs). Then, after complete freezing at −30 °C, the reaction mixtures followed a thawing step at 20 °C under vigorous agitation. The freezing/thawing process was repeated twice and the resulting solutions were maintained at 60 °C for 1 h (solvent evaporation technique), promoting physical gels formation. The residual alkali/urea solution was removed from hydrogels by exhaustive washing with Milli-Q water. Afterwards, prepared hydrogels were immersed in an ethanol solution (96%) for 3 days to extend and improve gels resistance [28].

After optimization of PI to Cs mass ratio, Cds were incorporated in the hydrogel's matrix, as follows: briefly, wet hydrogel (30 mg) was suspended in 10 mL of Cds solution (1–5 g/L) in dark at 5 °C for 48 h. The Cds entrapment efficiency (EE) and loading capacity (LC) by the hydrogels, defined as the quantity of loaded Cds per 100 g of hydrogels and the amount of loaded Cds based on the initial Cds, respectively, were determined considering the DTG thermograms, by subtracting the amount of Cds in the supernatant from the total amount applied [31]:

$$\text{Carotenoids LC (\%)} = \frac{\text{Mass of loaded carotenoids}}{\text{Mass of hydrogel samples}} \times 100 \quad (1)$$

$$\text{Carotenoids EE (\%)} = \frac{\text{Mass of loaded carotenoids}}{\text{Mass of initial carotenoids}} \times 100 \quad (2)$$

2.3.3. Hydrogels microstructure

The cross-section of Cs-PI composite hydrogels was observed using scanning electron microscopy SEM (Hitachi S4800), at an angle of 90° to the surface. Prior to imaging hydrogels cross-section, after being

sputter coated with a 5 nm thick gold, hydrogel samples were lyophilized, sectioned and fixed on the SEM support using a double side adhesive tape, and observed, under an accelerating voltage of 2.0 kV and an absolute pressure of 60 Pa.

2.3.4. Infrared spectroscopy analysis

The prepared Cs-based hydrogels FT-IR analysis was performed by means of a spectrometer (Agilent Technologies, Carry630 series) with an attenuated reflection accessory (ATR) containing a diamond/ZnSe crystal, at room temperature (25 °C). Spectra were recorded in the spectral range frequencies of 650–4000 cm^{-1}, with 32 scans of interferograms and a resolution of 4 cm^{-1}. Prior to analysis, FT-IR spectrometer was calibrated *via* a background spectrum recorded from the clean and empty diamond for each spectrum. Data analysis was carried out using the OMNIC Spectra software (ThermoFisher Scientific).

2.3.5. Physical properties of hydrogels

The water content was determined according to the methods described by the AOAC methods [24]. Weights before and after drying at 105 °C were measured. The water content was expressed in% (g moisture/100 g dry matter).

Regarding soluble peptides content of Cs-PI composite hydrogels, samples (0.5 g) were homogenized with 4.5 mL of 5% cold trichloroacetic acid TCA (4.5 mL) for 2 min. The mixtures were incubated for 1 h at 4 °C and then centrifuged at 8000 *g* for 10 min. The TCA-soluble peptide content in the supernatant was measured by the method of Lowry et al. [32] using L-tyrosine as a standard. The results are expressed in micromoles of tyrosine per gram of sample.

The swelling test was performed on pieces of hydrogels with masses of 20–30 mg. The samples were immersed in phosphate-buffered saline (PBS) at 37 °C and after 24 h of incubation, the samples were removed, oven-dried and the masses were measured again [33]. The swelling rate (SR) of Cs-based hydrogels, repeated three times, was calculated based on the following equation:

$$SR\ (\%) = \frac{M_s - M_d}{M_d} \times 100 \quad (3)$$

where SR is the swelling rate (%), M_d is the mass (g) of the oven-dried hydrogel and M_s is the mass (g) of the swollen hydrogel.

2.3.6. Thermal properties of blue crab chitosan-based hydrogels

Thermogravimetric analysis (TGA Q500 High Resolution, TA Instruments), operating under nitrogen flow, was used to study the thermal stability of hydrogels. The mass change of a sample as a function of temperature augmentation is the basis of TGA, and the progressive change in mass (%) as a function of temperature, is recorded. Hydrogels, initially about 4 mg, were heated from 25 to 700 °C at a heating rate of 20 °C/min and constantly measured with an accuracy of 0.01 mg. The Cs-based hydrogel thermograms were subsequently recorded, analyzed and treated using the TA Universal V4.5A software (TA Instruments, Waters, New Castle, UK).

Differential Scanning Calorimeter (Modulated DSC Q20, TA Instruments), equipped with a liquid nitrogen cooling system, was used to further investigate the thermal properties of hydrogels. Samples were accurately weighed into sealed aluminum pans. An empty capsule serves as an inert reference and the apparatus was calibrated using indium. The thermal profile was analyzed in a temperature range of 0–225 °C, at a heating rate scan of 10 °C/min, under nitrogen flow rate of 50 mL/min. Thermograms were then analyzed by using TA Universal V4.5A software.

2.3.7. Evaluation of hydrogels mechanical properties

Hydrogel compression tests were carried out using the DMA50 (Dynamic Mechanical Analyzer) universal testing machine (Metravib, Brand of ACOEM, France) at a temperature of 25 °C and a compression speed of 1 mm/min. Samples were compressed at 10%, 20%, 30%, 40%, 50% and 60%, and then reverted at the same speed of 1 mm/min, to obtain the stress-strain curves for gels' compression-recovery. The dimensions of the hydrogel specimens (parallelepiped) for compression tests were 10 mm × 5 mm × 5 mm (based on the apparatus requirements). The stress-strain curve hysteresis was treated by the instrument software.

2.3.8. Hydrogels in vitro degradation test

Hydrogels *in vitro* biodegradation study was monitored based on the gravimetric method described by Qu et al. [34]. Briefly, hydrogels (approximatively 100 mg) were immersed in 10 mL of phosphate buffer saline (PBS) at pH 7.4 (physiological microenvironment simulation) and 5.5 (acidic microenvironment), at 37 °C and under gentle shaking (~ 100 rpm). The rate of *in vitro* degradation, considering the remaining weight of hydrogels, after oven-drying during 48 h at 60 °C, was defined as %.

2.3.9. In vitro antioxidant activity and biocompatibility assessments of Cs-PI composite Cds loaded hydrogels

The *in vitro* antioxidative activity of Cs-PI composite hydrogels (aliquots of 10 mg) was evaluated based on the reducing power [35], DPPH radical scavenging [36] and metal chelating [37] *in vitro* assays.

The *in vitro* cytotoxicity of Cs-PI composite hydrogels was evaluated by the MTT assay [38]. Briefly, hydrogels were sterilized with ethanol for 30 min and under UV light (405 nm) for 1 h. MG-63 osteosarcoma cells, in logarithmic growth phase, were cultured on the sterilized hydrogels for 7 days. Cell viability was analyzed using the MTT assay. Cells were incubated with 100 µL of culture medium containing 0.05 mg/mL of MTT solution for 3 h. The obtained purple-colored formazan crystals, due to MTT reduction by living cells, were solubilized by addition of 100 µL of DMSO and optical density (OD) was recorded at 560 nm using a Multiskan microplate spectrophotometer (ThermoFisher, USA). 100 µL fresh medium was used as the negative control, and 100 µL phenol solution as the positive control. All experiments were carried out in triplicate. The cell viability was calculated from the OD values of the test sample and negative control using the following equation:

$$\text{Cell viability}\ (\%) = \frac{OD_{\text{test sample}}}{OD_{\text{negative control}}} \times 100 \quad (4)$$

2.4. In vitro drug release kinetics

In the present study, Cds were chosen as drug model for the drug delivery study. Briefly, Cds-loaded hydrogel samples (30 mg) were incubated in 10 mL of aqueous HCl-NaCl (0.1 M) solution with different pH values (pH 2.0, 4.5 and 7.4) at 37 °C, with stirring. At each time interval, an aliquot of the supernatant (2.5 mL) was withdrawn and replaced by fresh medium at the same volume. The released Cds amount was obtained considering the cumulative quantity of Cds in each of the release system, on the basis of a Cds calibration curve (Agilent Technologies UV–visible spectrometer, Carry 630 series) at 480 nm.

2.5. Wound healing in vivo potential of Cs-PI composite Cds-loaded hydrogels

2.5.1. Experimental design

In the present project, animals were divided into five groups of 6 rats each, as follows:

- **Group 1:** control rats receiving no treatment, only by cleaning with physiological serum;
- **Group 2:** rats receiving treatment with the reference MEBO®, (0.25% *w*/w β-sitosterol);

- **Group 3:** rats receiving treatment with Cs-based hydrogel patches;
- **Group 4:** rats treated with Cs-PI composite hydrogel patches (Supplementary data Fig. S1);
- **Group 5:** rats treated with Cs-PI composite Cds-loaded hydrogel patches (Supplementary data Fig. S2).

Before the induction of mechanical wounds with loss of substance, animals were razed with an electric razor and anesthetized by intramuscular injection of 50 mg/kg of ketamine. After immobilization, a wound of full thickness and area (1.5 cm × 1 cm) was induced using a pair of surgical scissors at the scapula, the dorsal region, inaccessible to scratching [39]. All the wounds were covered by sterilized compresses immediately.

Every two days, all wounds were cleaned with physiological serum. Then, each hydrogel sample was applied to the wounds. MEBO® reference healing drug was applied as a thin layer covering the entire surface of the wound. Treatments were stopped when complete wound healing occurred in all the animals of the same group. During the healing process experiments (13 days), wounds were regularly photographed and their surfaces were measured.

At the end of the experiments, the rats were anesthetized with ether, sacrificed and the granulation tissues were excised, for hydroxyproline content determinations (wet tissue immediately preserved at −80 °C) and for histological observations (tissue immediately fixed in formalin 10% (*v*/v)).

2.5.2. Quantitative study: wound area and contraction rate measurement

For the determination of wound area, wound boundaries were traced using transparent paper and area were measured with Autodesk AutoCAD 2014 ver. I.18.0.0 software application. The wound contraction rate was considering the below equation, as reported by Kirker et al. [40]:

$$\text{Wound contraction rate (\%)} = \frac{\text{initial surface } J_1 - \text{measured surface } J_i}{\text{initial surface } J_1} \times 100 \quad (5)$$

2.5.3. Biochemical study: hydroxyproline contents measurement

The determination of the hydroxyproline was carried out according to the method described by Edwards & O'Brien [41]. The 4-hydroxyproline released by acid hydrolysis is oxidized by chloramine T which transforms it into a pyrrole ring. The latter condenses, under heating, with para-dimethylamine benzaldehyde (PDMAB) to form a red compound which absorbs at 557 nm. Values were expressed as mg/g dry weight.

Collagen is a constitutional protein of the extracellular matrix of the skin consisting, in the cutaneous tissue, of hydroxyproline (about 13%). Thus, 4-hydroxyproline was used for the determination of the amount of collagen present in the neohealed tissue, according to the following formula [42]:

$$\text{Collagen content (mg g}^{-1}\text{ sample)} = \text{hydroxyproline content} \times 7.69 \quad (6)$$

2.5.4. Microscopic study: histologic examination approach

As abovementioned, on the last day of experiments, after animals' sacrifice, the excised tissue specimens, collected for histopathological examination purposes, were immediately fixed in neutral-buffered formalin (10%) and embedded in paraffin. Subsequently to cutting of paraffin (5 μm), hematoxylin–eosin was used to stain sections, to examine and photograph under a light microscope (Motic ME 2000, Hong Kong).

2.6. Statistical analysis

All experiments were carried out in triplicate and average values with standard deviation errors are reported. Mean separation and significance were analyzed using the SPSS software package ver. 17.0 professional edition (SPSS, Inc., Chicago, IL, USA) using ANOVA analysis. Differences were considered significant at $p < .05$.

3. Results and discussion

3.1. Blue crab protein isolate extraction and characterization

Chemical composition of freeze-dried sample was determined and showed that PI constituted a potential source of proteins (85.75 ± 1.65%) and low amounts of ash (8.19 ± 0.45%) and fats (1.52 ± 0.62%), based on the dried weight matter (Supplementary data Table S1). These findings were in line with previous studies reporting protein values in the range of 84.75% to 93.46% [43].

The extraction yield of the proteins, from the blue crab muscle, showed that extraction of the proteins by the pH-shifting approach made it possible to recover 18.44 ± 0.78% of proteins. Therefore, blue crab muscle with large amounts of proteins might be an adequate ingredient for the preparation of food for human consumption.

Solubility is a particularly important parameter for proteins, knowing that the functional properties of a macromolecule depend on its interactions with water, which is the major ingredient in most industrial formulations [44]. As a result, the solubility of PI in a pH range of 1.0 to 11.0 was studied at a concentration of 2% (Fig. 1A). The greatest protein solubility (> 80%) was observed at extreme acid (1.0–2.0) and alkaline (9.0–10.0) pH values. The lowest solubility (16.93 ± 1.17%) was noted at pH 5.0, close to the isoelectric pH of PI. Indeed, at extreme pHs, the number of positive or negative charges was important, favoring the repulsion of protein molecules and their interaction with water molecules. However, at a pH near the isoelectric point, the net charge of the protein was nil, which reduced the repulsion of the protein molecules by electrostatic forces and promoted their self-aggregation by hydrophobic forces [19].

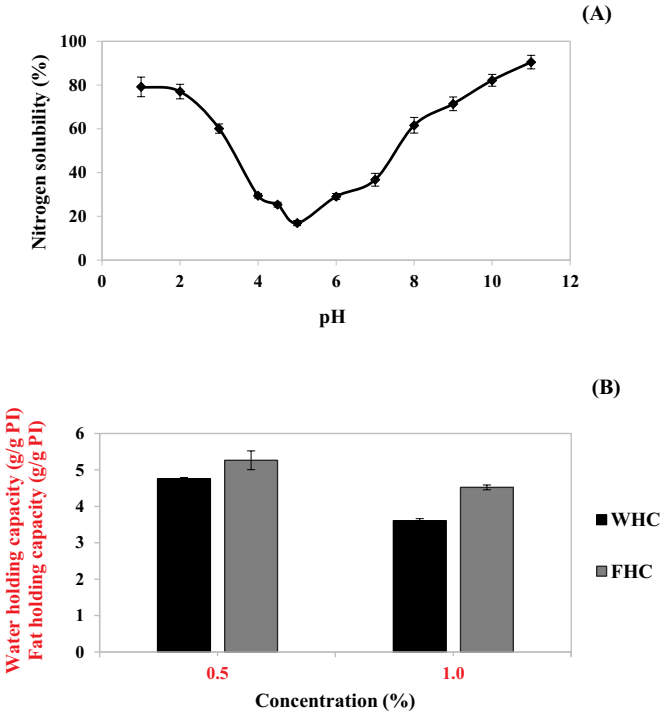

Fig. 1. Solubility at differents pH media (pH 1.0-pH 11.0) (A) and water holding/fat holding capacities (B) of PI at concentrations of 0.5 and 1% (*w*/*v*). PI: protein isolate from blue crab muscle; WHC: water holding capacity; FHC: fat holding capacity.

Table 1
Emulsifying activity EAI (m^2/ g) and emulsion stability ESI (min) index, Foam expansion FE (%) and foam stability FS (%) of PI at pH 2.0 and 11.0.

Emulsifying properties				
Concentration (%)	pH 2.0		pH 11.0	
	IAE (m^2/g)	ISE (min)	IAE (m^2/g)	ISE (min)
0.5	47.03 ± 0.94 ^{aB}	65.53 ± 0.67 ^{aA}	49.98 ± 0.67 ^{aA}	66.48 ± 1.26 ^{aA}
1	29.73 ± 1.78 ^{bB}	43.33 ± 2.68 ^{bA}	34.70 ± 1.52 ^{bA}	45.65 ± 2.1 ^{bA}
2	19.28 ± 1.01 ^{cB}	37.65 ± 1.25 ^{cA}	21.89 ± 0.62 ^{cA}	32.44 ± 2.07 ^{cB}
3	12.71 ± 0.67 ^{dA}	34.25 ± 1.35 ^{dA}	12.97 ± 0.17 ^{dA}	25.44 ± 0.23 ^{dB}
4	10.16 ± 0.02 ^{eA}	27.93 ± 0.1 ^{eA}	10.0 ± 0.05 ^{eA}	23.44 ± 0.17 ^{eB}
5	8.37 ± 0 ^{fB}	21.49 ± 0.72 ^{fA}	9.27 ± 0.06 ^{fA}	18.98 ± 0.13 ^{fB}

Foaming properties				
Concentration (%)	pH 2.0		pH 11.0	
	FE (%)	FS (%)	FE (%)	FS (%)
0.5	9.63 ± 0.68 ^{fB}	7.28 ± 0.56 ^{eB}	19.98 ± 0.67 ^{fA}	15.65 ± 0.81 ^{dA}
1	20.30 ± 0.96 ^{eB}	18.41 ± 0.67 ^{dB}	34.70 ± 1.52 ^{eA}	28.61 ± 1.2 ^{dA}
2	38.14 ± 0.85 ^{dB}	30.98 ± 1.02 ^{cB}	41.89 ± 0.62 ^{dA}	36.70 ± 0.72 ^{cA}
3	42.94 ± 1.09 ^{cB}	38.47 ± 1.12 ^{bA}	44.97 ± 0.67 ^{cA}	38.98 ± 1.09 ^{cA}
4	46.72 ± 0.93 ^{bB}	39.92 ± 0.97 ^{bB}	50.01 ± 0.32 ^{bA}	43.56 ± 0.48 ^{bA}
5	48.14 ± 0.42 ^{aB}	43.67 ± 0.85 ^{aB}	54.67 ± 0.58 ^{aA}	46.37 ± 1.03 ^{aA}

(a, f) Data with different letters in the same column indicate significant differences ($p < .05$) between the different concentrations of the PI.
(A, B) Data with different letters indicate significant differences ($p < .05$) between the different pH testing conditions.

Water (WHC) and fat (FHC) holding capacities are among the most important functional properties of proteins [45]. Obtained results (Fig. 1B) revealed that WHC and FHC depended on the concentration of PI. For example, at a concentration of 0.5%, PI could retain 4.76 g water/g PI, whereas this capacity decreased to 3.61 g water/g PI, at a concentration of 1%. Aletor et al. [46] described that WHC and FHC for applications in food or viscous products should be between 1.49 and 3.72 g/g PI and 1.49 to 4.17 g/g PI, respectively. Consequently, PI could be a potential ingredient in food or biotechnology applications requiring high water retention capacity or in viscous products.

The emulsifying property reflects the ability of a sample to adsorb rapidly at the oil/water interfaces when forming an emulsion by preventing flocculation and coalescence. The emulsifying activity EAI (m^2/ g) and emulsion stability ESI (min) index, at different concentrations (0.5–5%, *w/v*), are illustrated in Table 1. It is interesting to note that PI concentration seemed to significantly affect its emulsifying power. Indeed, at low protein concentrations, protein adsorption at the oil-water interface was controlled by diffusion. At higher concentrations, proteins had characteristic problems, including aggregation, precipitation, gelation and, in particular, increased viscosity, which may limit the protein-protein interactions necessary for the formation of the interfacial membrane around droplets of oil [47]. In another aspect, the IAE of IPs obtained under basic conditions (pH 11.0) was found to be significantly higher than that obtained at pH 2.0, which could be directly related to the solubility of the protein under these conditions [48,49].

Proteins cause in dispersions a lowering of the surface tension at the water/air interface, thus, creating foam. Foam expansion FE (%) and foam stability FS (%) of PI was, further, studied at various concentrations (0.5–5%, *w/v*) and results were depicted in Table 1. Results display that FE of PI significantly increased with the increasing of concentration, which could be the result of a higher rate of diffusion of foam properties with molecule concentration [50]. However, at all concentrations studied, FS decreased significantly with time.

3.2. Design and optimization of blue crab chitosan-protein isolate composite hydrogels

The present research concerns a process for the development of hydrogels, based Cs and PI, with enhanced mechanical properties. In fact, the strategy of polymers blending, most of the time easier to implement, making it possible to develop new materials with improved properties.

3.2.1. Study of Cs-PI composite hydrogels structural features

According to one embodiment, the microstructures of the cross-sections of Cs-PI composite hydrogels were studied by SEM in comparison with reference hydrogel based on Cs 100% (Fig. 2). Based on the obtained micrographs, it was observed that the incorporation of PI into the hydrogel matrix resulted in a change in their microstructure. In fact, as expected, the pore size in the hydrogels decreased with the increase of the added amount of PI, due to the increase in the cross-linking density [30].

FT-IR spectra of Cs-PI composite hydrogels were studied (Fig. 3A). The profile of G-Cs_100% revealed typical Cs absorption bands at wavenumbers 3417 cm^{-1}, 1627 cm^{-1}, 1544 cm^{-1}, 1407 cm^{-1} and 1020–1097 cm^{-1} ascribed to the –OH, Amide *I* groups (-C=O), Amide II (-NH_2), –CH and glycoside rings, respectively [21]. For composite hydrogels, Cs absorbance and other protein distinguishing peaks were detected, located at 1641–1623 cm^{-1} (Amide I) associated with a carbonyl elongation vibration (-C=O) at the level of the peptide bonds, 1546 cm^{-1} (Amide II) due to an elongation vibration of the -NH bond and to an extensional vibration of the -CN bond at the level of the peptide bonds, 1251 cm^{-1} (Amide III) assigned to a combination of previous vibrations with deformation vibrations of –CH_2 groups. The addition of PI to the Cs-based hydrogel formulation induced an increase in the intensity of Amide A (Fig. 3A), indicating, therefore, the formation of intermolecular hydrogen bonds between proteins and Cs [51]. In addition, the decrease in the frequency of Amide II gels (from 1552 cm^{-1} to 1546 cm^{-1}), as a function of the concentration of PI, suggested the presence of changes in the conformation of the polypeptide chains of PI [52]. This change could be related to amino and carbonyl groups, which interact primarily through electrostatic interactions [53].

3.2.2. Cs-PI composite hydrogels physical properties

Cs-PI composite hydrogels revealed a water content of around 88%

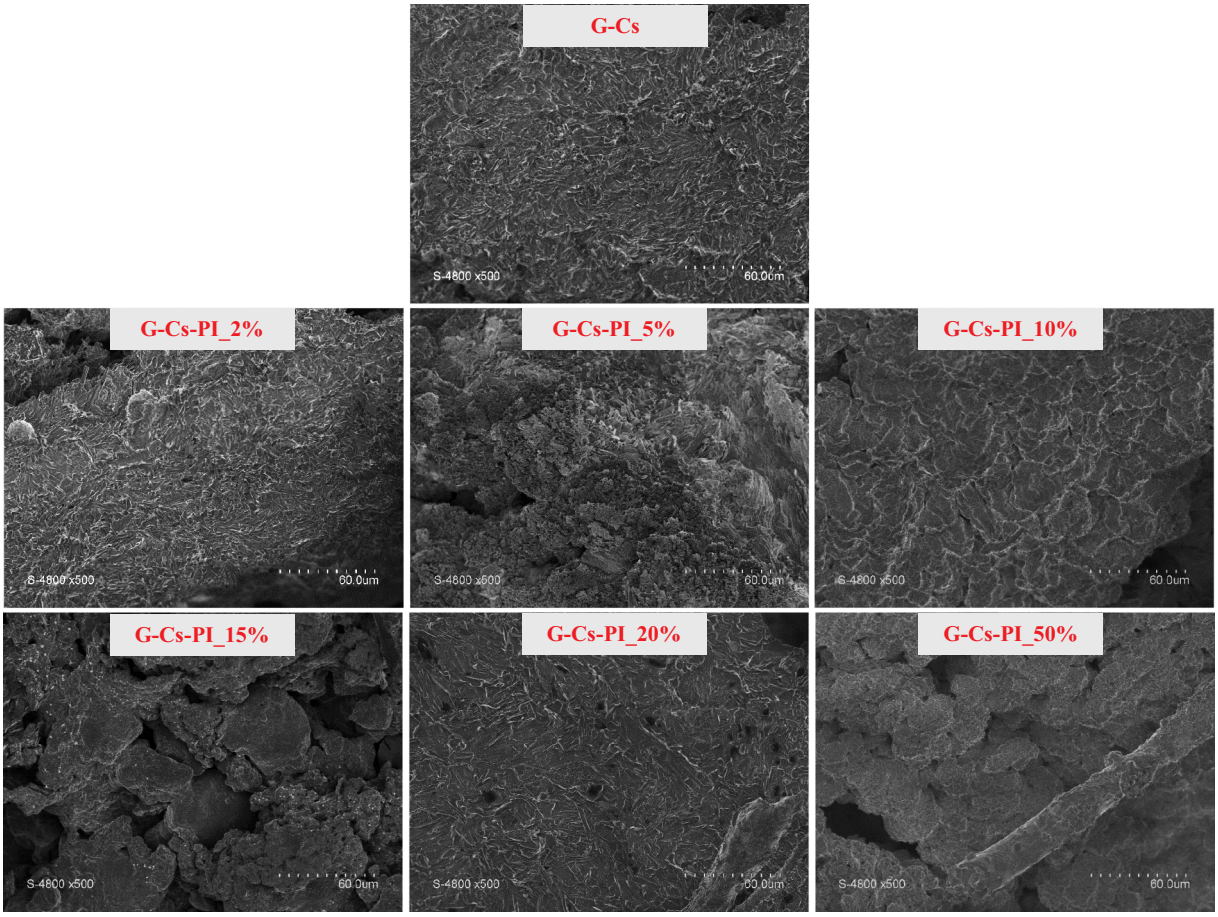

Fig. 2. SEM images of Cs-PI composite hydrogels cross-sections. G: hydrogel; Cs: chitosan from blue crab shells; PI: protein isolate from blue crab muscle.

(Table 2). The water content is one of the parameters that differentiate hydrogels from other biomaterials. Their water-rich structure facilitates the transport of nutrients and molecules between the external environment and the gel, allowing to mimic cells function in the body [54].

The addition of PI in the matrix of hydrogel not exceeding 15% (*w*/w Cs) improved ($p < .05$) its water retention capacity (WRC), which was enhanced from 18 g water/100 g gel (G-Cs_100%) to 31 g water/100 g gel (G-Cs-PI_15%). Nevertheless, beyond this concentration, a significant decrease in WRC was noted, to 14% for G-Cs-PI_50% ($p < .05$), significantly lower ($p < .05$) than that of G-Cs_100% (Table 2). Generally, different water retention capacities indicated expressible moisture differences in the gel network, suggesting an increase in breaking strength [19]. Thus, Cs-PI composite hydrogels at a concentration not exceeding 15% (w/w Cs) could be characterized by the lowest water release capacity, and probably the hardest hydrogel network.

Moreover, the content of soluble peptides in hydrogels (Table 2) was found to be PI concentration dependent. In fact, G-Cs-PI_2% exhibited the lowest soluble peptide content (17.71 μmol tyr/g gel) compared to that of G-Cs-PI_10% (22.14 μmol tyr/g gel), G-Cs-PI_20% (29.11 μmol tyr/g gel) and G-Cs-PI_50% (39.90 μmol tyr/g gel) ($p < .05$). It is interesting to note that peptides were present in the control hydrogel prepared with 100% Cs (15.73 μmol tyr/g gel), probably resulting from traces of residual peptides in the Cs macromolecular chains.

As an absorbent matrix, the SR of a hydrogel is a key parameter that is closely related to the ability of the system to release active ingredients. Results show that SR of hydrogels was proportional to PI concentration (Table 2). Indeed, G-Cs_100% displayed SR of only 18 g water/g gel, compared to G-Cs-PI_ 50% with SR of 32 g water/g gel ($p < .05$). It is, thereby, possible to deduce that the addition of PI promoted an increase and an improvement in the hydrophilic nature of the gels, favoring their interactions with the water molecules. In addition to the polarity of the hydrogels, the degree of crosslinking or porosity was correlated with the ability of the hydrogels to absorb water [55,56].

3.2.3. *Investigation of hydrogels thermal properties*

For their application in the pharmaceutical industries, the study of thermal properties of hydrogels is essential [57]. With the addition of PI to the Cs solution, a corresponding reduction in degradation temperatures was observed, in a PI dose-dependent manner (Fig. 3B), indicating, thereby, a reduction in the mobility of Cs molecular chains subsequent to their interaction with PI [58].

Thermal analysis of Cs-PI composite hydrogels shows no additional intermediate degradation peak, suggesting the biocompatibility between Cs and the myofibrillar proteins of PI. Subsequently, the incorporation of PI made it possible to integrate with the polymeric network of Cs, forming, thereby, a copolymer (Cs-PI) more resistant to thermal degradation than the Cs alone, in terms of weight loss (Fig. 3B). Regarding the residual mass, it was found that the residual quantity of hydrogels increased with the increase in PI concentration, with respective values of 52.47%, 56.84% and 62.1% for G-Cs-PI_5%, G-Cs-PI_10% and G-Cs-PI_15% *vs.* 42.84% for the control G-Cs_100%. Nevertheless, at concentrations of 20% and 50% (*w*/w Cs) of PI, the residual mass decreased to 59.47% and 53.87%, respectively. Thus, the thermal stability of composite gels was positively correlated with the amount of added PI not exceeding 15% (w/w Cs).

In another aspect of the study of Cs-PI composite hydrogels thermal

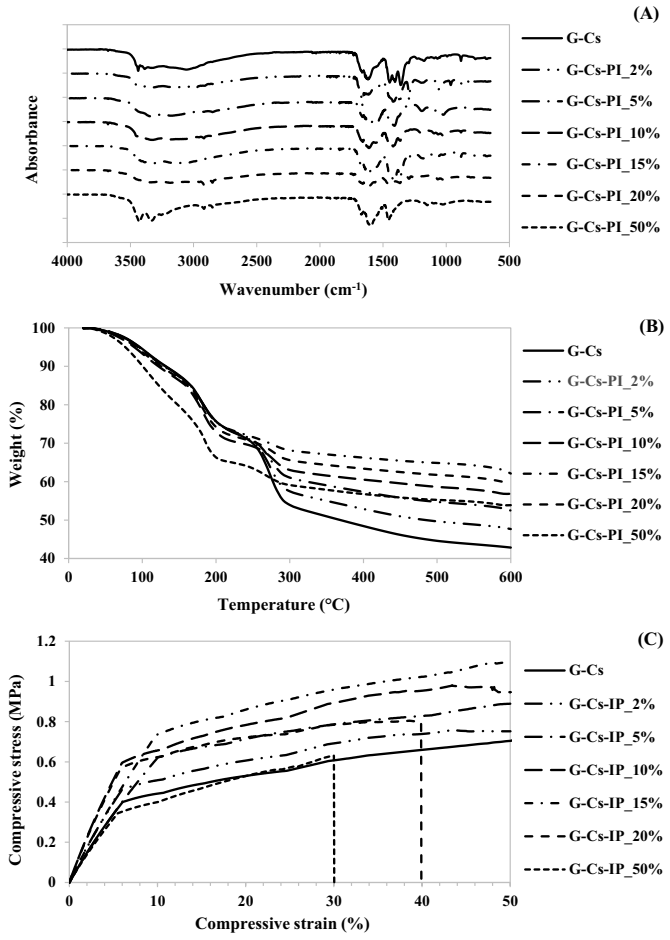

Fig. 3. FT-IR spectra of Cs-PI composite hydrogels cross-sections (A). ATG thermograms of Cs-PI composite hydrogels cross-sections (B). Mechanical behavior of Cs-PI composite hydrogels cross-sections, in terms of compressive stress *vs.* compressive strain curves (C). G: Hydrogel; Cs: chitosan from blue crab shells; PI: protein isolate from blue crab muscle.

properties, considering DSC analysis, the glass transition temperature (Tg) was determined (Table 2). G-Cs_100% revealed a Tg of 42 °C. The incorporation of PI allowed an improvement of the intermediate Tg values for composite hydrogels at PI concentrations not exceeding 15% (w/w Cs). Indeed, Tg values of 41.93 °C, 42.50 °C, 42.75 °C and 43.58 °C were noted for PI concentrations of 2%, 5%, 10% and 15% (w/w Cs), respectively. Nevertheless, at added amounts of PI of 20% and 50% (w/w Cs), Tg values decreased to 42.81 °C and 42.38 °C, respectively. Independently of the obtained values, only one Tg was advantageously detected, testifying, subsequently, to the good compatibility between the Cs and PI. Accordingly, Cs and PI were miscible and the rigidity of the resulting mixture gels decreased with the increase of PI content exceeding 15%.

3.2.4. *Cs-PI composite hydrogels mechanical behavior*

The exposition of wet gels to compression testing was studied, to have additional insight into the mechanical behavior of Cs-PI composite hydrogels, and the compression stress *vs.* strain diagrams are illustrated in Fig. 3C. Experimental outcomes display that the application of a compressive force on the hydrogels resulted in bi-phasic curves. At low deformation values (< 5%), an elastic (reversible) deformation, shown in the diagram by a straight line (deformation proportional to the stress), was observed. Up to 5% compression strain, the stress augmented sluggishly, subsequently a plastic deformation (irreversible), due to the bonds breaking or structure rearrangement, demonstrating that the Cs-based hydrogels were robust and pliable [59,60].

The study of the mechanical behavior of hydrogels in a compression regime show that G-Cs-PI_15% was the most resistant to deformation (1.10 MPa), followed by G-Cs-PI_10% (0.95 MPa) *vs.* 0.70 MPa for the control G-Cs_100%, as reported in Fig. 3C ($p < .05$). Conversely, G-Cs-PI_20% and G-Cs-PI_50% lost their elasticity, exhibiting stress of 0.80 MPa and 0.62 MPa ($p < .05$), respectively, which can be attributed to the decrease in brittleness due to excess of polymers' chains entanglement [56,61]. The present work demonstrated thus a good ability of PI to strengthen the Cs hydrogels, mainly related to the contribution of the myofibrillar proteins of the PI particularly that of actomyosin. Knowing that hydrogels elasticity highly affected their biomedical potential applications, synthetized Cs-PI composite hydrogels, with promoting mechanical behavior could be applied as an interesting alternative biomaterial for tissue engineering [6,10].

3.2.5. *Assessment of the stability against in vitro degradation of Cs-PI composite hydrogels*

To simulate the physiological and acidic microenvironments, PBS pH 5.5 and pH 7.4 were used to evaluate the *in vitro* degradation behavior of Cs-PI composite hydrogels, considering their weight loss (Fig. 4A and B, respectively). Results reveal that hydrogels stability decreased with the incubation period as evidenced by the gradual diminution of the remaining weights, probably due to gels' surface and internal erosion [62,63], to variable extend ($p < .05$) in terms of PI concentration. Compared to samples immersed in PBS pH 7.4, hydrogels in PBS pH 5.5 displayed a more rapid *in vitro* degradation profile ($p < .05$). During 4 days of swelling in a physiological-like microenvironment (PBS pH 7.4), G-Cs_100% and G-Cs-PI_50% retained >

Table 2
Physicochemical characterization, in terms of humidity (%), water retention capacity (WRC, %), soluble peptides content (μmoles tyr/g gel) and swelling rate SR (g water/g gel) and *in vitro* antioxidant activities of Cs-PI composite hydrogels.

	G-Cs_100%	G-Cs-PI_2%	G-Cs-PI_5%	G-Cs-PI_10%	G-Cs-PI_15%	G-Cs-PI_20%	G-Cs-PI_50%	G-Cs-PI Cds
Humidity (%)	81.87 ± 1.02 ^{b}	87.15 ± 1.01 ^{a}	87.88 ± 0.71 ^{a}	88.13 ± 0.06 ^{a}	88.75 ± 0.96 ^{a}	89.03 ± 0.61 ^{a}	89.51 ± 1.06 ^{a}	ND
WRC (%)	18.03 ± 0.12 ^{e}	20.10 ± 1.09 ^{d}	24.21 ± 0.44 ^{c}	28.35 ± 0.71 ^{b}	31.08 ± 0.60 ^{a}	22.37 ± 0.67 ^{d}	14.97 ± 1.13 ^{f}	ND
Soluble peptides (μmoles tyr/g)	15.73 ± 0.37 ^{f}	17.71 ± 0.28 ^{e}	18.95 ± 0.44 ^{e}	22.14 ± 0.36 ^{d}	25.36 ± 0.52 ^{c}	29.11 ± 0.46 ^{b}	39.90 ± 1.36 ^{a}	ND
SR (g/g)	18.10 ± 0.47 ^{g}	19.74 ± 0.21 ^{f}	21.51 ± 0.71 ^{e}	25.41 ± 0.39 ^{d}	27.55 ± 0.84 ^{c}	29.90 ± 0.93 ^{b}	32.56 ± 1.01 ^{a}	ND
Tg (°C)	41.56	41.93	42.50	42.75	43.58	42.81	42.38	ND
Cs-PI composite hydrogels antioxidant activities								
DPPH radical scavenging (%)	93.47 ± 1.37 ^{e}	95.93 ± 0.08 ^{d}	96.87 ± 0.84 ^{c}	99.04 ± 0.13 ^{b}	100 ± 0.0 ^{a}	100 ± 0.0 ^{a}	100 ± 0.0 ^{a}	100 ± 0.0 ^{a}
Metal chelating (%)	88.73 ± 1.94 ^{f}	90.14 ± 1.12 ^{f}	92.78 ± 0.93 ^{e}	94.10 ± 0.08 ^{d}	95.24 ± 0.11 ^{c}	97.33 ± 0.35 ^{b}	100 ± 0.0 ^{a}	100 ± 0.0 ^{a}
Reducing power (OD_{700} nm)	0.119 ± 0.01 ^{g}	0.133 ± 0.03 ^{g}	0.179 ± 0.01 ^{f}	0.272 ± 0.01 ^{e}	0.493 ± 0.01 ^{d}	0.573 ± 0.01 ^{c}	0.782 ± 0.02 ^{b}	1.13 ± 0.12 ^{a}

(a, g) Data with different letters in the same row indicate significant differences ($p < .05$) between the different concentrations of the PI added to the Cs-based hydrogels. G: Hydrogel; G-Cs-PI Cds: Cs-PI composite loaded Cds (4 g/L); ND: not determined.

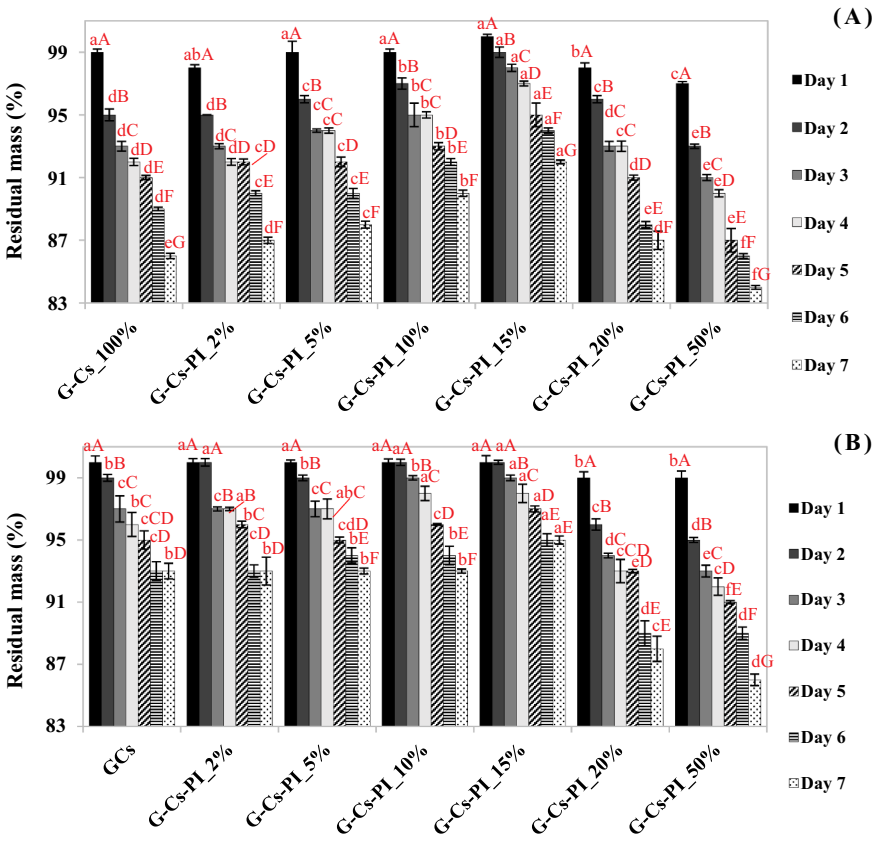

Fig. 4. *In vitro* biodegradation of Cs-PI composite hydrogels in PBS (phosphate buffered saline) at pH 5.5 (acidic microenvironment) (A) and pH 7.4 (physiological microenvironment simulation) at 37 °C (B). [(a, f)] Data with different letters in the same swelling day indicate significant differences ($p < .05$) between the different hydrogels as function of PI added concentration. [(A, G)] Data with different letters indicate significant differences ($p < .05$) between the different swelling days for the same hydrogel.

95% and 92% of their masses, respectively (Fig. 4B) *vs.* about 92% and 90% in PBS pH 5.5, respectively (Fig. 4A), which could be attributed to the result of pH influence on the Cs and PI interaction strength [34].

Moreover, as expected, composite hydrogels exhibited a better stability against *in vitro* degradation until a PI concentration not exceeding 15% (Fig. 4A and B). Residual weights of approximately 93% for G-Cs-PI_2%, G-Cs-PI_5% and G-Cs-PI_10% and about 95% for G-Cs-PI_15% were reached, whereas, G-Cs-PI_20% and G-Cs-PI_50% maintained only 88% and 86% of their initial weight, respectively, after 7 days of swelling in PBS pH 7.4, at 37 °C ($p < .05$) (Fig. 4B). The same tendency was noted after swelling under acidic conditions, with PBS pH 5.5 at 37 °C (Fig. 4A). These outcomes corroborated well with the pore diameter distribution based on the SEM images, the swelling, mechanical and thermal behaviors of the synthetized Cs-PI composite hydrogels [64,65].

Independently of the swelling conditions, > 83% of Cs-PI composite hydrogels initial mass was preserved (Fig. 4A and B). Overall, all these results suggested that Cs-PI composite hydrogels endowed good stability in PBS, and could present a potential and promising application in tissue engineering [66].

3.2.6. Cs-PI composite Cds loaded hydrogels in vitro antioxidant activity

Results illustrating the antioxidant properties of Cs-PI composite hydrogels, compared to the bare Cs-based hydrogels, are shown in Table 2. None a sole antioxidative mechanism could be sufficient to justify overall biomaterials antioxidant potential, which could be ascribed to the cooperative effects of these systems, such as metal chelation and scavenging radicals [67]. Independently of the investigated antioxidant systems, reached values were markedly higher ($p < .05$) with Cs-PI composite hydrogels than with pure Cs-based hydrogels. The different synthetized hydrogels were able of stabilizing the DPPH free radicals and reducing ferric ions (Fe^{3+}), also endowed with a very interesting iron ions chelating power, regardless the PI added concentration, but in a PI quantity-dependent manner. Indeed, DPPH free radicals and iron ions chelating activities of 100% were reached with G-Cs-PI_50% *vs.* 93% and 88%, respectively, for Cs-based hydrogel non reinforced with PI. Furthermore, considering the case of the reducing power assessment, the OD_{700} increased > 4- and almost 6-folds in the presence of 15% and 50% of PI (*w*/w Cs), *vs.* OD_{700} of 0.119 for the unadded Cs-based hydrogel.

As abovementioned in FT-IR analysis, and based on microstructure features perceived by SEM, this finding could be explained, not only, by the increase of the amount of polypeptides and bioactive peptides and the enhancement of free amino groups availability in the composite hydrogels, but also, to favorable surface morphology permitting positive circumstances for free radicals scavenging [68]. Therefore, the incorporation of PI to Cs-based hydrogel matrix network improved the antioxidant activity of the resultant hydrogels.

Moreover, the significantly high antioxidant potential ($p < .05$) of the designed Cs-PI composite Cds-loaded hydrogel could be further ascribed to Cds components, characterized as having high carotenoids content (mainly astaxanthin), and exhibiting distinguished antioxidant activity [22].

3.2.7. Study of the biocompatibility of Cs-PI composite hydrogels

In order to examine the biocompatibility of Cs-PI composite hydrogels, the growth behavior of MG-63 cells, that were derived from a human bone osteosarcoma and exhibit osteogenic potential, on the hydrogel surface was studied. Fig. 5 reveals the relative viability of cells cultured on the hydrogel surface by MTT assay. Compared with cells grown without hydrogels (control), the statistical analysis displayed no significant differences in the viability of the cells in the presence of Cs-based hydrogel (G-Cs) and Cs-PI composite hydrogel at a concentration of 5% (*w*/w Cs) of PI ($p > .05$). Additionally, it can be perceived that at a concentration of PI not exceeding 15% (w/w Cs), the cell viability for the composite hydrogel groups was > 80% ($p > .05$), compared to the Cs-based hydrogel non added with PI ($p > .05$), after a cells culture time of 7 days (Fig. 5), indicating the well proliferation of the MG-

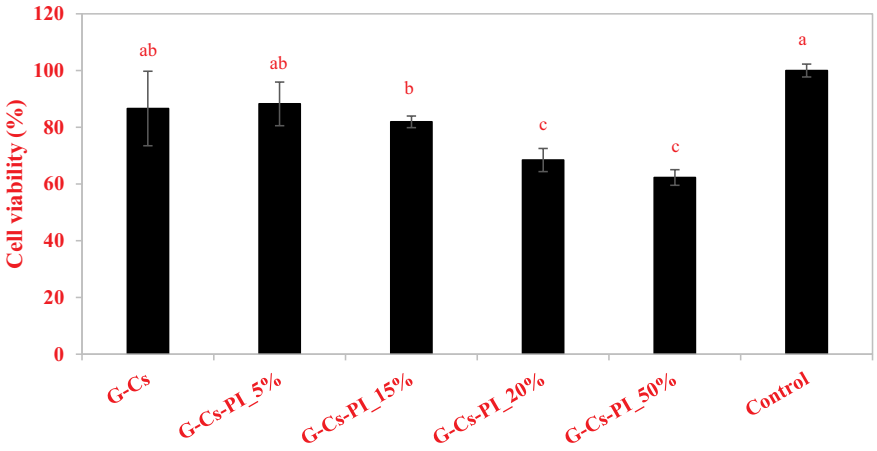

Fig. 5. MG-63 osteosarcoma cells viability, when cultured in the presence of Cs-PI composite hydrogels. Hydrogels biocompatibility was assessed with the MTT assay at 7 after seeding. Data are presented as the mean ± sd (n = 3). [a, c] Data with different letters in the same swelling day indicate significant differences ($p < .05$) between the different hydrogels as function of PI added concentration.

63 cells on the prepared hydrogel surfaces. These findings suggest that PI incorporation as crosslinker for Cs, at concentrations not exceeding 15% (w/w Cs) was biocompatible. However, the cell proliferation significantly decreased ($p < .05$) to an average of > 60% for Cs-PI composite hydrogel groups at concentrations of 20% and 50% (w/w Cs) of PI (Fig. 5).

Altogether, these results suggest that Cs-based hydrogels regenerated in ethanol solution exhibited remarkable biocompatibility and with reduced cytotoxicity. Moreover, Cs-PI composite hydrogels at PI amounts not exceeding 15% (w/w Cs) could serve as substrates for cell growth for application in tissue engineering or wound healing.

3.3. *In vitro drug release*

Innovative drug delivery systems, with the ability of liberating their active components in response to environmental stimuli, were, nowadays, established thanks to chitosan hydrogels advanced progresses [59,69]. As a drug model, the kinetics of Cds release, *via* the synthetized Cs-PI composite hydrogels, was monitored on the basis of the cumulative Cds released quantities as a function of time (Fig. 6).

Considering its fitting structural features, swelling behavior and mechanical strength, G-Cs-PI_15% was designated for the study of the *in vitro* Cds release kinetics.

Foremost, Cs-PI composite hydrogels EE and LC towards Cds was assessed and it was clearly noted their dependence to Cds concentration ($p < .05$). In fact, EE values increased from > 75% for 1 g/L Cds to approximately 89% for 4 g/L Cds, respectively (Fig. 6A). However, above a concentration of 4 g/L of Cds, the EE values dropped with 5 g/L Cds to reach ~ 70%. This was in line with the LC results with respective values of 24%, 32% and 37% for 1 g/L, 2 g/L and 3 g/L Cds. After swelling in 4 g/L and 5 g/L Cds solutions, no significant differences were noted ($p > .05$), with respective LC values of 41% and 40%.

Regarding the Cds release kinetics study, Cs-PI composite hydrogels exhibited a delivery scheme of Cds, in HCl-NaCl (0.1 M) pH 5.5, characterized by an initial short rapid release, followed by low Cds release, which tended to stabilize after 72 h (Fig. 6B). The primary release rates were 19% for Cds concentrations of 1 g/L, after 8 h of swelling time, 49% after 24 h and 85% at the end of the study (4 days). At a Cds concentration of 5 g/L, 11%, 19% and 32% of initial loaded Cds were released after, 8 h, 24 h and 96 h. In terms of the total mass of Cds released, at a Cds concentration of 1 g/L, the amount of released Cds was 850 mg after 96 h, while at 5 g/L of Cds, > 1.6 g of Cds were released, testifying that the overall release behavior of synthetized hydrogels was greatly related and dependent to Cds concentration, attributed to higher Cds concentration gradient with the increase of Cds loading, as a diffusion modulating force [34].

Considering a concentration of 4 g/L, Cds delivery behavior were further assessed in HCl-NaCl (0.1 M) medium, at different pH (2.0, 4.5 and 7.4) and at 37 °C (Fig. 6C). As expected, resulting curves show that Cds were not markedly liberated from the synthetized hydrogels at pH 7.4. However, a significantly distinguished released amount ($p < .05$) was noted in more acidic microenvironments (pH 4.5), mainly at pH 2.0 microenvironment, with the highest and fastest rate, probably due to the exhaustive destruction of the hydrogel structure, which was in accordance with the *in vitro* degradation outcomes [33]. Indeed, after 96 h of a swelling reaction-time, in a Cds solution of 4 g/L, releasing rates of 91%, 81% and 15%, for pH 2.0, pH 4.5 and pH 7.4, respectively.

The obtained Cds release schemes suggested that synthetized Cs-PI composite hydrogels could be applied as pH-sensitive intelligent porous biomaterials for drugs-controlled deliverance, with sufficient space for their diffusion. Additionally, thanks to their structural organization, swelling behavior and appropriate pliability, Cs-PI composite hydrogels seemed to be a very interesting biomaterial for tissue engineering perspectives [64].

3.4. *In vivo wound healing assessments in Wistar rats*

It is well known that one of the common issues, requiring to be well-thought-out, is skin injury, which is the major body organ critically handling maintaining its function. Indeed, skin behaves as water excess evaporation and microorganisms' diffusion to internal organs preventer or barrier [70]. Accordingly, and since skin healing is a complex phenomenon, advanced developments in tissue engineering has drown more and more attention to hydrogels as appropriate and interesting scaffolds for tissue regeneration [71].

Based on the above described outcomes, considering the structural features, swelling behavior and mechanical strength of Cs-PI composite hydrogels, G-Cs-PI_15% loaded or not with 4 g/L of Cds was designated for the study of the wound healing *in vivo* potential of hydrogel-based patches, and compared to Cs-based hydrogel patches (G-Cs_100%) and the wound healing reference (MEBO).

3.4.1. *Wound healing qualitative evaluation*

Optical images of wounds repair during 13 days of experiment for all treatments were presented in Fig. 7A. At the beginning of the experiment (just after injury), all wounds showed a similar appearance and a bright red color, which persists even at the third postoperative day in untreated rats, as evidenced by the wound bed optical images analysis (Fig. 7A).

From the fifth day of post-wounding care, the aspects of the wounds instigated to discriminate. In fact, rats treated with synthetized hydrogels (groups 3, 4 and 5) revealed a brown color of the wounds, compared to those of the reference (group 2) and control (group 1) groups, with noted perilesional redness. On the seventh day of the experimental study, inflammation reaction around the damaged skin of

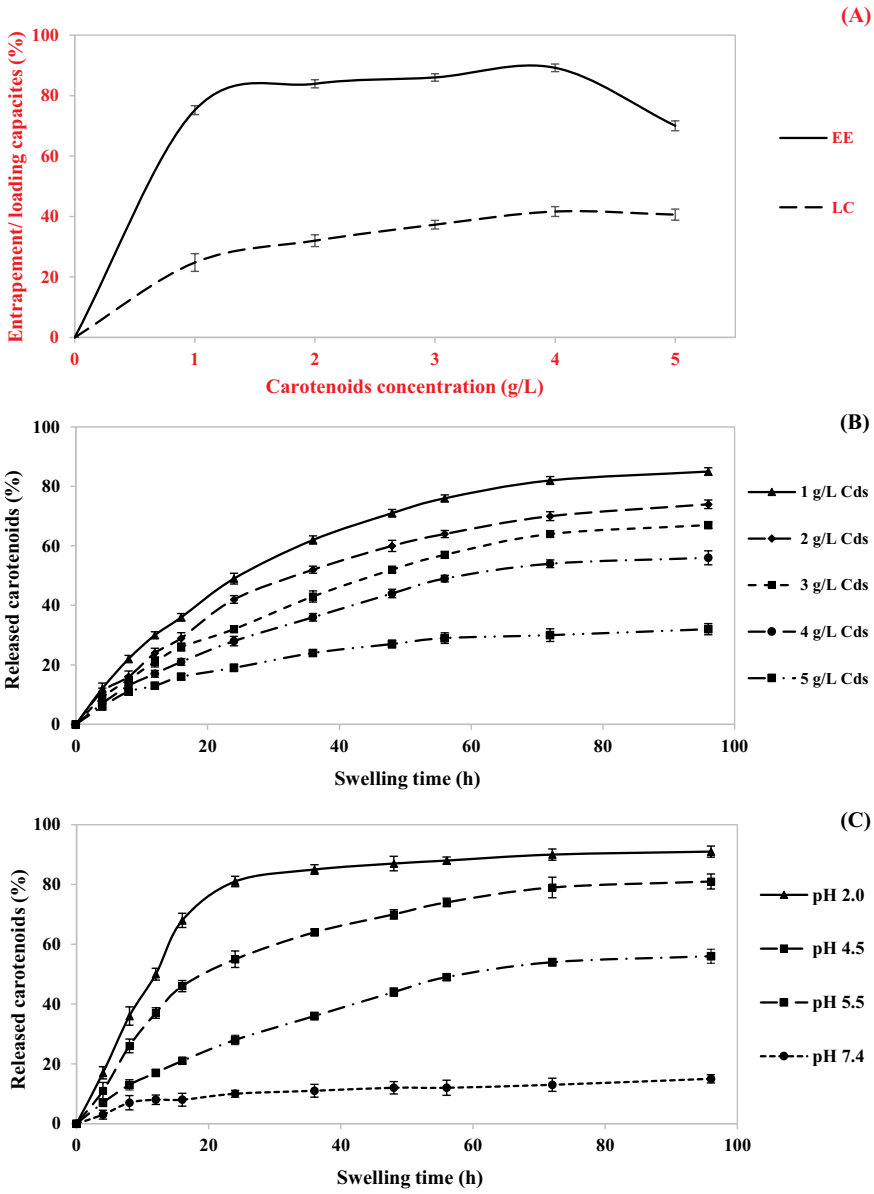

Fig. 6. Carotenoids entrapment efficiency (EE) and loading charge (CC) of the Cs-PI composite hydrogels, at a concentration of 3% (w/v) of Cs and an added amount of 15% (*w*/w) of PI (A).Profile and kinetics of *in vitro* release of carotenoids, as a drug model, from Cs-PI composite hydrogels. The incorporation of carotenoids was monitored by immersion in a solution of carotenoids (0–5 g/L) in the dark and at 5 °C for 48 h. The release assays were performed in HCl/NaCl (0.1 M) with different pH values (pH 2.0, pH 4.5 and pH 7.4) at 37 °C. Kinetics of cumulative release of carotenoids at different concentrations (0–5 g/L carotenoids) at pH 5.5 (B). Kinetics of cumulative release of carotenoids (4 g/L) at different pH values 2.0, 4.5 and 7.4 (C). Cds: carotenoids from blue crab shells; EE: entrapment efficiency; LC: loading capacity.

untreated wounds was detected, ergo an extended inflammation. Mild inflammation occurrence at wound healing initial phases is beneficial, allowing the induction of wound healing, while, strong and enduring inflammation could disadvantageously disturb the healing phenomenon progression [8]. However, a brown color scab was observed in the treated groups (testing and reference lots), which was found to be thicker and rather stiffer in rats treated with the standard wound healing drug and rats treated with Cs-PI composite Cds loaded hydrogel, compared with Cs-based and Cs-PI composite hydrogels treated animals' groups. This scab persisted in all rats' groups treated with hydrogels until the ninth day of the wound healing experiment (Fig. 7A).

From the eleventh day, scabs in rats treated with patches based on Cs-PI composite hydrogels, in particular loaded with Cds, began to drop to reveal a pinkish colored tissue. Moreover, unlike the reference (some wounds of the reference group remained open) and the untreated (unhealed wounds at the end of the experiment), utmost of the scabs of rats treated with synthetized hydrogels-based patches fell off, revealing unsoiled, healthy and pinkish color wounds (Fig. 7A). This accelerated epithelialization efficiency of the synthetized hydrogels, mainly, Cs-PI composite Cds loaded hydrogel, in wound healing could be ascribed to Cs and Cds synergetic antioxidant effects [21,22]. Similar observations were reported in other previous studies in the field of tissue regeneration [64,72,73].

3.4.2. *Wounds area and contraction rate measurements*

In another aspect of the wound healing experiments, the average areas of the wounds (Supplementary data Table S2) and the average contraction percentages of their surfaces (Fig. 7B), as important parameters to be considered in wound healing assessment, were determined. It could be clearly noted that the topical application of the tested engineered hydrogels and the wound healing reference MEBO were found capable of hastening the healing dynamics.

Compared to all rats in the other groups, delayed healing was observed in control rats' group treated only with physiological serum (group 1), in terms of wound closure and the healing contraction. Interestingly, after a 13-day treatment, wound contraction was complete in rats treated with Cs-PI composite Cds loaded hydrogel, exhibiting better healing performance, compared to Cs-PI composite hydrogel (97%), Cs-based hydrogel (93%) and MEBO (91%) treated animals ($p < .05$). However, the wound closure of the control group was of 87% ($p < .05$).

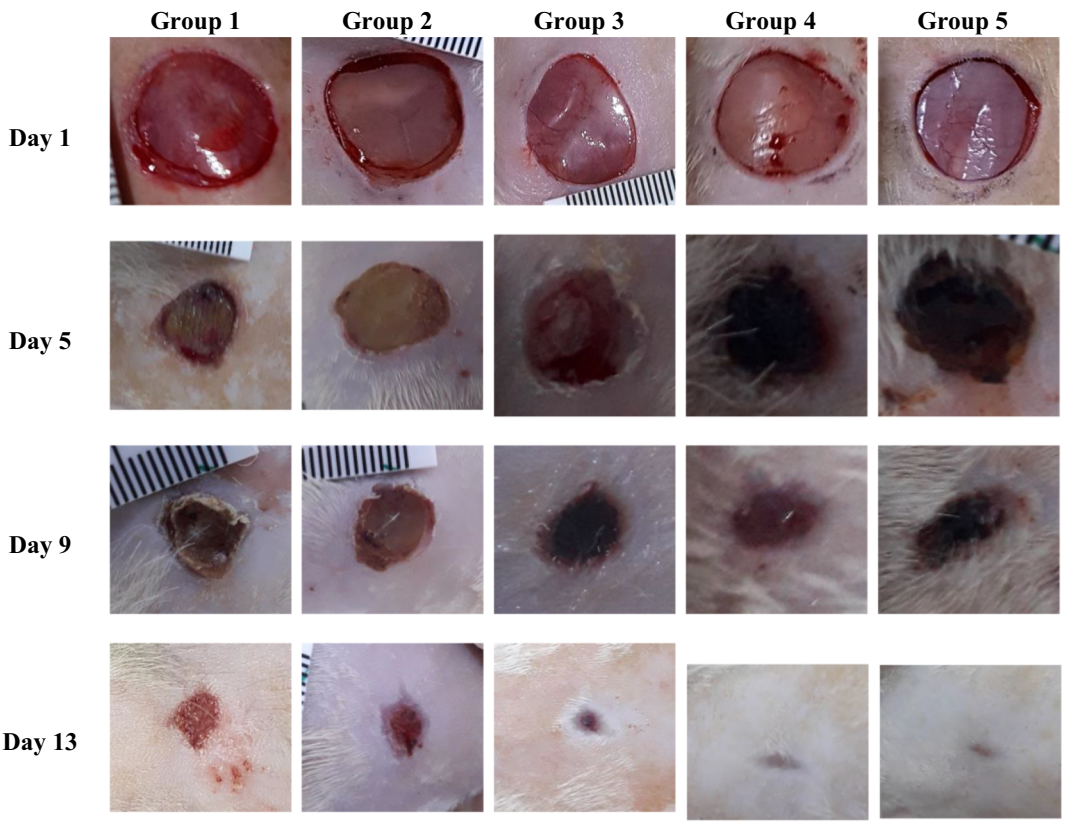

Fig. 7. Photographs of mechanical wounds of the five groups during the wound healing treatment period (A). Evolution of the average of wounds contraction percentages of the five groups studied (B). Average collagen concentrations of rat groups at the end of the wound healing experiments (C). Group 1: control rats treated with physiological serum; Group 2: rats treated with the MEBO® healing reference; Group 3: rats treated with Cs-based hydrogel patches; Group 4: rats treated with Cs-PI composite hydrogel patches; Group 5: rats treated with Cs-PI composite Cds-loaded hydrogel patches. [(a, c)] Data with different letters indicate significant differences ($p < .05$) between the different groups of animals.

Similarly, Jafari et al. [6] described that thermal-crosslinkable chitosan/maleic terminated polyethylene glycol hydrogels exhibited accelerated wound closure, with improved vascularization. Otherwise, accelerated cell proliferation, epithelization and infections reduction resulted from the increase of wound contraction. Accordingly, our findings proved that engineered hydrogels, specially Cs-PI composite Cds loaded hydrogel, could be considered as effective wound-healing biomaterials, ascribed to Cs ability and efficiency to improve cell proliferation, and thereby, hasten epithelialization, ergo accelerated wound healing.

3.4.3. Determination of hydroxyproline and collagen contents

The present study concerns, further, the determination of hydroxyproline concentration, and thereby the contents of collagen, the structural protein of the extracellular connective tissue (Fig. 7C). The concentration of collagen in all scar tissues in the treated groups, regardless of the formulation, was found to be distinctly superior to that of the untreated control group ($p < .05$). In the scar tissue treated with Cs-PI composite Cds loaded hydrogel, the collagen concentration was significantly higher (578 mg/g), followed by Cs-PI composite hydrogel treated animals (470 mg/g), compared to other groups ($p < .05$). No significant differences in the collagen content were noted, with respective values of 232 mg/g, 266 mg/g and 219 mg/g, for rats receiving Cs-based hydrogel, MEBO and physiological serum treatments.

The increase in collagen content is the result of more hydroxyproline deposition, biochemical specific indicator of the content of collagen in tissue. The evaluation of collagen production alteration revealed that synthetized hydrogels contributed effectively to the wound healing acceleration process in the damaged tissue, probably *via* exodus of fibroblasts into the damaged region, providing a connective tissue network [74].

3.4.4. Histologic approach for wound healing microscopic examination

As aforementioned, cutaneous tissue healing is a multifaceted and composite phenomenon, histological evaluation is a compelling approach to reinforce and assess wound healing, based on sections of areas hematoxylin-eosin staining, in terms of collagen and fibroblast contents, re-epithelization and neovascularization, deposition of inflammatory cells, collagen and fibroblasts [64]. Therefore, at the thirteen day of experiment (end of the assessment), granulation tissues for both hydrogels and control groups were excised and histologically evaluated (Fig. 8).

Overall experiment, biopsies of physiological serum treated group (group 1), showed still prearranged and incomplete re-epithelization. However, well-patterned and orchestrated dermis, with well-differentiated epidermal layers and a complete healed tissue, were detected with the MEBO reference (group 2) and the prepared hydrogels treated (groups 3, 4 and 5) groups (Fig. 8). This could be attributed to wound surface closure which was essential to engender a hypoxic wound environment and stimulate the neovascularization [5,6]. Interestingly, group 5 (Cs-PI composite Cds-loaded hydrogel treated rats) displayed the establishment of new blood vessel and thin epidermal layer allied

(B)

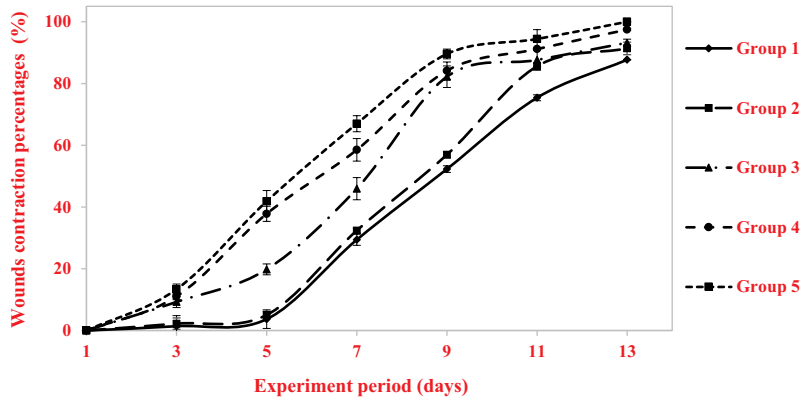

(C)

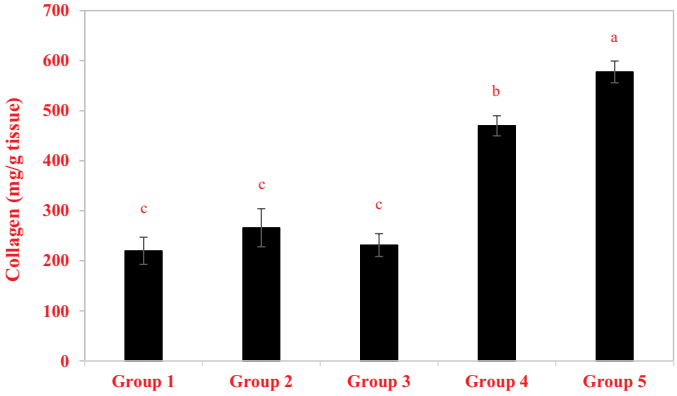

Fig. 7. (*continued*)

with less inflammatory cell infiltration in the wound area, testifying of complete healing, in an orchestrated fashion, close to the normal skin tissue at the end of the wound healing experiment (Day 13). The anti-inflammatory effects of Cs and Cds could explain these findings, suggesting that Cs-based biomaterial promoted and controlled the growth factors responsible for cell proliferation and differentiation [75].

Conversely, group 1 (untreated) disclosed an imperfect regeneration, hyperemia of capillary blood vessel and active inflammatory lesion related with inflammatory cell infiltration in the underlying tissue, mainly plasma, lymphocytes cells, and macrophages, marked by small round nuclei strongly colored in purple (Fig. 8). This is in line with abovementioned results regarding the hydroxyproline content in the granulation tissue biopsies, indicating the lowest collagen density. Besides tissue reconstruction, wound healing is critically affected by the deposition, distribution, and alignment in wound area of collagen, synthesized by fibroblast cells, that can accelerate epithelialization, and thereby, the wound healing process. Rat groups treated with MEBO and engineered Cs-based hydrogels revealed the attendance of connective tissue related to the vigorous improvement in the organization and deposition of collagen fibers (Fig. 8), that can promote and accelerate the wound healing cascade, endorsing tissue reform [68].

Consequently, the histologic evaluation emphasized an appropriate epithelial remodeling in the Cs-PI composite Cds-loaded hydrogel treated group, with an enhancement of the wound-healing process, by stimulating fibroblast proliferation, with perfect connective tissues reorganization and a homogenous dense architecture. Similar studies reported that Cs, among other biopolymers-based scaffolds, improved the collagen and fibroblast formation, and decreased the number of inflammatory cells, which enhanced the wound healing process [57,72,76].

4. Conclusion

In the present study, composite hydrogels based on blue crabs' Cs and PI were developed and enriched with carotenoids extracted from the same species. The results of our investigation show that PI, at a concentration not exceeding 15%, played an interesting role in improving Cs-based hydrogels structural, swelling, mechanical and *in vitro* stability and antioxidant properties, with low cytotoxicity towards MG-63 osteosarcoma cells. The obtained release patterns displayed that composite hydrogels could be applied as a smart pH-sensitive carrier for controlled drug-delivery for further biomedical applications. When used for wound healing treatment in rats, hydrogels, particularly Cs-PI composite Cds-loaded hydrogel, accelerated wound closure with enhanced angiogenesis, showing that these hydrogels are promising candidates to treat skin injuries and damages.

Marwa Hamdi: Conceptualization, Methodology, Validation, Formal analysis, Investigation, Writing - original draft, Visualization.**Amal Feki:**Investigation.**Sana Bardaa:**Investigation.**Suming Li:**Resources, Supervision.**Sakthivel Nagarajan:**Investigation.**Manel Mellouli:**Investigation.**Tahia Boudawara:**Supervision.**Zouheir Sahnoun:**Supervision. **Moncef Nasri:**Resources, Supervision, Writing - review & editing.**Rim Nasri:**Resources, Supervision.

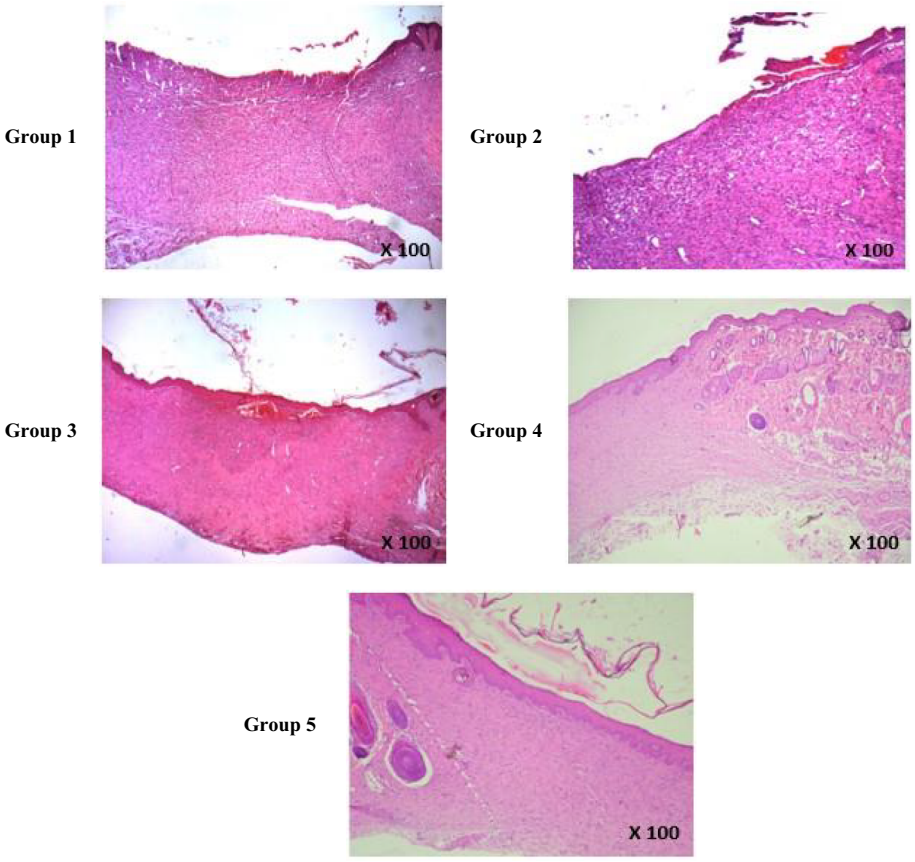

Fig. 8. Photomicrographs of histologic sections of cutaneous scabs (x 40) at day 13 of the experiment treatment (hematoxylin-eosin staining). Group 1: control rats treated with physiological serum; Group 2: rats treated with the MEBO® healing reference; Group 3: rats treated with Cs-based hydrogel patches; Group 4: rats treated with Cs PI composite hydrogel patches; Group 5: rats treated with Cs-PI composite Cds-loaded hydrogel patches.

Acknowledgement

The present work was funded by the Ministry of Higher Education and Scientific Research, Tunisia.

References

[1] B. Tavsanli, O. Okay, Mechanically robust and stretchable silk/hyaluronic acid hydrogels, Carbohydr. Polym. 208 (2019) 413–420.
[2] Z. Shariatinia, Pharmaceutical applications of chitosan, Adv. Colloid Interf. Sci. 263 (2019) 131–194.
[3] T.M. Aminabhavi, S.P. Dharupaneedi, Production of chitosan-based hydrogels for biomedical applications, Chitosan Based Biomaterials Volume 1 – Fundamentals, 2017, pp. 295–319.
[4] A. Rehman, Q. Tong, S.M. Jafari, E. Assadpour, Q. Shehzad, R.M. Aadil, M.W. Iqbal, M.M.A. Rashed, B.S. Mushtaq, W. Ashraf, Carotenoid-loaded nanocarriers: a comprehensive review, Adv. Colloid Interf. Sci. 275 (2020) 102048.
[5] X. Du, Y. Liu, X. Wang, H. Yan, L. Wang, L. Qu, D. Kong, M. Qiao, L. Wang, Injectable hydrogel composed of hydrophobically modified chitosan/oxidized-dextran for wound healing, Mater. Sci. Eng. C 104 (2019) 109930.
[6] A. Jafari, S. Hassanajili, N. Azarpira, M.B. Karim, B. Geramizadeh, Development of thermal-crosslinkable chitosan/maleic terminated polyethylene glycol hydrogels for full thickness wound healing: *In vitro* and *in vivo* evaluation, Eur. Polym. J. 118 (2019) 113–127.
[7] P.S. Patil, N. Fountas-Davis, H. Huang, M.M. Evancho-Chapman, J.A. Fulton, L.P. Shriver, N.D. Leipzig, Fluorinated methacrylamide chitosan hydrogels enhance collagen synthesis in wound healing through increased oxygen availability, Acta Biomater. 36 (2016) 164–174.
[8] K. Ravishankar, M. Venkatesan, R.P. Desingh, A. Mahalingam, B. Sadhasivam, R. Subramaniyam, R. Dhamodharan, Biocompatible hydrogels of chitosan-alkali lignin for potential wound healing applications, Mater. Sci. Eng. C 102 (2019) 447–457.
[9] S. Kim, Z.K. Kui, B. Koo, J. Zheng, T. Aghaloo, M. Lee, Chitosan–lysozyme conjugates for enzyme-triggered hydrogel degradation in tissue engineering applications, ACS Appl. Mater. Interfaces 10 (2018) 41138–41145.
[10] E. Patois, S. Osorio-da Cruz, J.C. Tille, B. Walpoth, R. Gurny, O. Jordan, Novel thermosensitive chitosan hydrogels: *in vivo* evaluation, J. Biomed. Mater. Res. A 91 (2009) 324–330.
[11] S.A. Agnihotri, N.N. Mallikarjuna, T.M. Aminabhavi, Recent advances on chitosan-based micro- and nanoparticles in drug delivery, J. Control. Release 100 (2004) 5–28.
[12] M. Hamdi, S. Hajji, S. Affes, W. Taktak, H. Maâlej, M. Nasri, R. Nasri, Development of a controlled bioconversion process for the recovery of chitosan from blue crab (*Portunus segnis*) exoskeleton, Food Hydrocoll. 77 (2018) 534–548.
[13] V. Patrulea, V. Ostafe, G. Borchard, O. Jordan, Chitosan as a starting material for wound healing applications, Eur. J. Pharm. Biopharm. 97 (2015) 417–426.
[14] Y. Tu, N. Chen, C. Li, H. Liu, R. Zhu, S. Chen, Q. Xiao, J. Liu, S. Ramakrishna, L. He, Advances in injectable self-healing biomedical hydrogels, Acta Biomater. 90 (2019) 1–20.
[15] J. Berger, M. Reist, A. Chenite, O. Felt-Baeyens, J.M. Mayer, R. Gurny, Pseudo-thermosetting chitosan hydrogels for biomedical application, Int. J. Pharm. 288 (2005) 197–206.
[16] T. Dai, G.P. Tegos, M. Burkatovskaya, A.P. Castano, M.R. Hamblin, Chitosan acetate bandage as a topical antimicrobial dressing for infected burns, Antimicrob. Agents Chemother. 53 (2009) 393–400.
[17] S.P. Noel, H.S. Courtney, J.D. Bumgardner, W.O. Haggard, Chitosan sponges to locally deliver amikacin and vancomycin: a pilot in vitro evaluation, Clin. Orthop. Relat. Res. 468 (2010) 2074–2080.
[18] W. Xu, Z. Wang, Y. Liu, L. Wang, Z. Jiang, T. Li, W. Zhang, Y. Liang, Carboxymethyl chitosan/gelatin/hyaluronic acid blended-membranes as epithelia transplanting scaffold for corneal wound healing, Carbohydr. Polym. 192 (2018) 240–250.
[19] W. Taktak, R. Nasri, M. Hamdi, L.G. Gomez-Mascaraque, A. Lopez-Rubio, S. Li, M. Nasri, M. Chaabouni, Physicochemical, textural, rheological and microstructural properties of protein isolate gels produced from European eel (*Anguilla anguilla*) by heat-induced gelation process, Food Hydrocoll. 82 (2018) 278–287.
[20] G. Labib, Overview on zein protein: a promising pharmaceutical excipient in drug delivery systems and tissue engineering, Expert Opinion on Drug Delivery 15 (2017) 65–75.
[21] M. Hamdi, R. Nasri, S. Hajji, M. Nigen, S. Li, M. Nasri, Acetylation degree, a key

parameter modulating chitosan rheological, thermal and film-forming properties, Food Hydrocoll. 87 (2019) 48–60.
[22] M. Hamdi, R. Nasri, N. Dridi, H. Moussa, L. Ashour, M. Nasri, Improvement of the quality and the shelf life of reduced-nitrites turkey meat sausages incorporated with carotenoproteins from blue crabs shells, Food Control 91 (2018) 148–159.
[23] M. Chaijan, W. Panpipat, S. Benjakul, Physicochemical and gelling properties of short-bodied mackerel (*Rastrelliger brachysoma*) protein isolate prepared using alkaline-aided process, Food Bioprod. Process. 88 (2010) 174–180.
[24] AOAC, Official Methods of Analysis, 17th ed., Association of Official Analytical Chemists, Washington, DC, 2000.
[25] F. Soxhlet, Die gewichtsanalytische bestimmung des milchfettes, Dinglers Polytechnisches Journal 232 (1879) 461–465.
[26] K. Tsumura, T. Saito, K. Tsuge, H. Ashida, W. Kugimiya, K. Inouye, Functional properties of soy protein hydrolysates obtained by selective proteolysis, LWT Food Sci. Technol. 38 (2005) 255–261.
[27] M.J.Y. Lin, E.S. Humbert, F.W. Sosulski, Certain functional properties of sunflower meal products, J. Food Sci. 39 (1974) 368–370.
[28] F. Shahidi, X.Q. Han, J. Synowiecki, Production and characteristics of protein hydrolysates from capelin (*Mallotus villosus*), Food Chem. 53 (1995) 285–293.
[29] K.N. Pearce, J.E. Kinsella, Emulsifying properties of proteins: evaluation of a turbidimetric technique, J. Agric. Food Chem. 26 (1978) 716–723.
[30] J. Duan, X. Liang, Y. Cao, S. Wang, L. Zhang, High strength chitosan hydrogels with biocompatibility via new avenue based on constructing nanofibrous architecture, Macromolecules 48 (2015) 2706–2714.
[31] B. Huang, M. Liu, C. Zhou, Chitosan composite hydrogels reinforced with natural clay nanotubes, Carbohydr. Polym. 175 (2017) 689–698.
[32] O.H. Lowry, N.J. Rosebrough, A.L. Farr, R.J. Randall, Protein measurement with the Folin phenol reagent, J. Biol. Chem. 193 (1951) 265–275.
[33] S. Yu, X. Zhang, G. Tan, L. Tian, D. Liu, Y. Liu, X. Yang, W. Pan, A novel pH-induced thermosensitive hydrogel composed of carboxymethyl chitosan and poloxamer cross-linked by glutaraldehyde for ophthalmic drug delivery, Carbohydr. Polym. 155 (2017) 208–217.
[34] J. Qu, X. Zhao, P.X. Ma, B. Guo, pH-responsive self-healing injectable hydrogel based on N-carboxyethyl chitosan for hepatocellular carcinoma therapy, Acta Biomater. 58 (2017) 168–180.
[35] A. Yildirim, A. Mavi, A.A. Kara, Determination of antioxidant and antimicrobial activities of *Rumex crispus* L. extracts, J. Agric. Food Chem. 49 (2001) 4083–4089.
[36] P. Bersuder, M. Hole, G. Smith, Antioxidants from a heated histidine-glucose model system. I: investigation of the antioxidant role of histidine and isolation of antioxidants by high-performance liquid chromatography, J. Am. Oil Chem. Soc. 75 (1998) 181–187.
[37] E.A. Decker, B. Welch, Role of ferritin as a lipid oxidation catalyst in muscle food, J. Agric. Food Chem. 38 (1990) 674–677.
[38] W. Zhang, M. Torabinejad, Y. Li, Evaluation of cytotoxicity of MTAD using the MTT-Tetrazolium method, J. Endod. 29 (2003) 654–657.
[39] L.A. Dipietro, A.L. Burns, Wound Healing: Methods and Protocols, Humana, 2003.
[40] K.R. Kirker, Y. Luo, J.H. Nielson, J. Shelby, G.D. Prestwich, Glycosaminoglycan hydrogel films as bio-interactive dressings for wound healing, Biomaterials 23 (2002) 3661–3671.
[41] C.A. Edwards, W.D. O'Brien Jr., Modified assay for determination of hydroxyproline in a tissue hydrolyzate, Clin. Chim. Acta 104 (1980) 161–167.
[42] J. Kale, J. Darwin, Modified procedure for the assay of H 3-or C 14-labeled hydroxyproline, Anal. Biochem. 15 (1966) 77–83.
[43] L. Najafian, M. Jafarzade, M. Said, A.S. Babji, Biochemical properties and antioxidant activity of myofibrillar protein hydrolysates obtained from patin (*Pangasius sutchi*), Int. J. Food Sci. Technol. 48 (2013) 2014–2022.
[44] P. Hou, F. Pu, H. Zou, M. Diao, C. Zhao, C. Xi, T. Zhang, Whey protein stabilized nanoemulsion: a potential delivery system for ginsenoside Rg3 whey protein stabilized nanoemulsion: potential Rg3 delivery system, Food Biosci. 31 (2019) 100427.
[45] M. Chalamaiah, B. Dinesh Kumar, R. Hemalatha, T. Jyothirmayi, Fish protein hydrolysates: proximate composition, amino acid composition, antioxidant activities and applications: a review, Food Chem. 135 (2012) 3020–3038.
[46] O. Aletor, A. Oshodi, K. Ipinmoroti, Chemical composition of common leafy vegetables and functional properties of their leaf protein concentrates, Food Chem. 78 (2002) 63–68.
[47] I. Jemil, M. Jridi, R. Nasri, N. Ktari, R. Ben Slama-Ben Salem, M. Mehiri, M. Hajji, M. Nasri, Functional, antioxidant and antibacterial properties of protein hydrolysates prepared from fish meat fermented by Bacillus subtilis A26, Process Biochem. 49 (2014) 963–972.
[48] A. Moure, H. Domínguez, J.C. Parajó, Antioxidant properties of ultrafiltration-recovered soy protein fractions from industrial effluents and their hydrolysates, Process Biochem. 41 (2006) 447–456.
[49] S. Benelhadj, A. Gharsallaoui, P. Degraeve, H. Attia, D. Ghorbel, Effect of pH on the functional properties of Arthrospira (*Spirulina*) platensis protein isolate, Food Chem. 194 (2016) 1056–1063.
[50] C.C. Sanchez, J.M.R. Patino, Interfacial, foaming and emulsifying characteristics of sodium caseinate as influenced by protein concentration in solution, Food Hydrocoll. 19 (2005) 407–416.
[51] N.G. Voron'ko, S.R. Derkach, Y.A. Kuchina, N.I. Sokolan, The chitosan–gelatin (bio) polyelectrolyte complexes formation in an acidic medium, Carbohydr. Polym. 138 (2016) 265–272.
[52] S.F. Hosseini, M. Rezaei, M. Zandi, F. Farahmandghavi, Fabrication of bio-nanocomposite films based on fish gelatin reinforced with chitosan nanoparticles, Food Hydrocoll. 44 (2015) 172–182.
[53] M. Pereda, A.G. Ponce, N.E. Marcovich, R.A. Ruseckaite, J.F. Martucci, Chitosan-gelatin composites and bi-layer films with potential antimicrobial activity, Food Hydrocoll. 25 (2011) 1372–1381.
[54] R. Dimatteo, N.J. Darling, T. Segura, *In situ* forming injectable hydrogels for drug delivery and wound repair, Adv. Drug Deliv. Rev. 127 (2018) 167–184.
[55] A.M. Heimbuck, T.R. Priddy-Arrington, B.J. Sawyer, M.E. Caldorera-Moore, Effects of post-processing methods on chitosan-genipin hydrogel properties, Mater. Sci. Eng. C 98 (2019) 612–618.
[56] Z. Huang, C. Gao, Y. Huang, X. Zhang, X. Deng, Q. Cai, Injectable polyphosphazene/gelatin hybrid hydrogel for biomedical applications, Mater. Des. 160 (2018) 1137–1147.
[57] Y. Xie, X. Liao, J. Zhang, F. Yang, Z. Fan, Novel chitosan hydrogels reinforced by silver nanoparticles with ultrahigh mechanical and high antibacterial properties for accelerating wound healing, Int. J. Biol. Macromol. 119 (2018) 402–412.
[58] Y.H. Cheng, T.H. Tsai, Y.Y. Jhan, A.W.H. Chiu, K.L. Tsai, C.S. Chien, S.H. Chiou, C.J.L. Liu, Thermosensitive chitosan-based hydrogel as a topical ocular drug delivery system of latanoprost for glaucoma treatment, Carbohydr. Polym. 144 (2016) 390–399.
[59] X. Chen, M. Fan, H. Tan, B. Ren, G. Yuan, Y. Jia, J. Li, D. Xiong, X. Xing, X. Niu, X. Hu, Magnetic and self-healing chitosan-alginate hydrogel encapsulated gelatin microspheres via covalent cross-linking for drug delivery, Mater. Sci. Eng. C 101 (2019) 619–629.
[60] Y.R. Choi, E.H. Kim, S. Lim, Y.S. Choi, Efficient preparation of a permanent chitosan/gelatin hydrogel using an acid-tolerant tyrosinase, Biochem. Eng. J. 129 (2018) 50–56.
[61] W. Huang, Y. Wang, Z. Huang, X. Wang, L. Chen, Y. Zhang, L. Zhang, On-demand dissolvable self-healing hydrogel based on carboxymethyl chitosan and cellulose nanocrystal for deep partial thickness burn wound healing, ACS Appl. Mater. Interfaces 10 (2018) 41076–41088.
[62] R. Song, J. Zheng, Y. Liu, Y. Tan, Z. Yang, X. Song, S. Yang, R. Fan, Y. Zhang, Y. Wang, A natural cordycepin/chitosan complex hydrogel with outstanding self-healable and wound healing properties, Int. J. Biol. Macromol. 134 (2019) 91–99.
[63] X. Liang, J. Duan, Q. Xu, X. Wei, A. Lu, L. Zhang, Ampholytic microspheres constructed from chitosan and carrageenan in alkali/urea aqueous solution for purification of various wastewater, Chem. Eng. J. 317 (2017) 766–776.
[64] Y. Song, N. Nagai, S. Saijo, H. Kaji, M. Nishizawa, T. Abe, *In situ* formation of injectable chitosan-gelatin hydrogels through double crosslinking for sustained intraocular drug delivery, Mater. Sci. Eng. C 88 (2018) 1–12.
[65] F. Wahid, X.H. Hu, L.Q. Chu, S.R. Jia, Y.Y. Xie, C. Zhong, Development of bacterial cellulose/chitosan based semi-interpenetrating hydrogels with improved mechanical and antibacterial properties, Int. J. Biol. Macromol. 122 (2019) 380–387.
[66] Y. Liang, M. Wang, Z. Zhang, G. Ren, Y. Liu, S. Wu, J. Shen, Facile synthesis of ZnO QDs@GO-CS hydrogel for synergetic antibacterial applications and enhanced wound healing, Chem. Eng. J. 378 (2019) 122043.
[67] N. Zhang, H. Chen, Y. Zhang, L. Ma, X. Xu, Comparative studies on chemical parameters and antioxidant properties of stipes and caps of shiitake mushroom as affected by different drying methods, J. Sci. Food Agric. 93 (2013) 3107–3113.
[68] H. Wang, X. Gong, X. Guo, C. Liu, Y.Y. Fan, J. Zhang, B. Niu, W. Li, Characterization, release, and antioxidant activity of curcumin-loaded sodium alginate/ZnO hydrogel beads, Int. J. Biol. Macromol. 121 (2019) 1118–1125.
[69] A. Rasool, S. Ata, A. Islam, Stimuli responsive biopolymer (chitosan) based blend hydrogels for wound healing application, Carbohydr. Polym. 203 (2019) 423–429.
[70] H. Fang, J. Wang, L. Li, L. Xu, Y. Wu, Y. Wang, X. Fei, J. Tian, Y. Li, A novel high-strength poly(ionic liquid)/PVA hydrogel dressing for antibacterial applications, Chem. Eng. J. 365 (2019) 153–164.
[71] R. Jangde, S. Srivastava, M.R. Singh, D. Singh, *In vitro* and *In vivo* characterization of quercetin loaded multiphase hydrogel for wound healing application, Int. J. Biol. Macromol. 115 (2018) 1211–1217.
[72] A. Ehterami, M. Salehi, S. Farzamfar, H. Samadian, A. Vaez, S. Ghorbani, J. Ai, H. Sahrapeyma, Chitosan/alginate hydrogels containing alpha-tocopherol for wound healing in rat model, Journal of Drug Delivery Science and Technology 51 (2019) 204–213.
[73] V. Patrulea, L.A. Laurent-Applegate, V. Ostafe, G. Borchard, O. Jordan, Polyelectrolyte nanocomplexes based on chitosan derivatives for wound healing application, Eur. J. Pharm. Biopharm. 140 (2019) 100–108.
[74] S. Bardaa, N. Chabchoub, M. Jridi, D. Moalla, M. Mseddi, T. Rebai, Z. Sahnoun, The effect of natural extracts on laser burn wound healing, J. Surg. Res. 201 (2016) 464–472.
[75] J. Pan, Y. Jin, S. Lai, L. Shi, W. Fan, Y. Shen, An antibacterial hydrogel with desirable mechanical, self-healing and recyclable properties based on triple-physical crosslinking, Chem. Eng. J. 370 (2019) 1228–1238.
[76] A. Feki, I. Ben Amara, S. Bardaa, S. Hajji, N. Chabchoub, R. Kallel, T. Boudawara, S. Zghal, R. Ben Salah, M. Nasri, N. Ktari, Preparation and characterization of polysaccharide-based films and evaluation of their healing effects on dermal laser burns in rats, Eur. Polym. J. 115 (2019) 147–156.